analytical chemistry

Article

pubs.acs.org/ac

Redox Couples with Unequal Diffusion Coefficients: Effect on Redox Cycling

Dileep Mampallil, Klaus Mathwig, Shuo Kang, and Serge G. Lemay*

MESA+ Institute for Nanotechnology, University of Twente, P.O. Box 217, 7500 AE Enschede, The Netherlands

ABSTRACT: Redox cycling between two electrodes separated by a narrow gap allows dramatic amplification of the faradaic current. Unlike conventional electrochemistry at a single electrode, however, the mass-transport-limited current is controlled by the diffusion coefficient of both the reduced and oxidized forms of the redox-active species being detected and, counterintuitively, by the redox state of molecules in the bulk solution outside the gap itself. Using a combination of finite-element simulations, analytical theory, and experimental validation, we elucidate the interplay between these interrelated factors. In so doing, we generalize previous results obtained in the context of scanning electrochemical microscopy and obtain simple analytical results that are generally applicable to experimental situations where efficient redox cycling takes place.

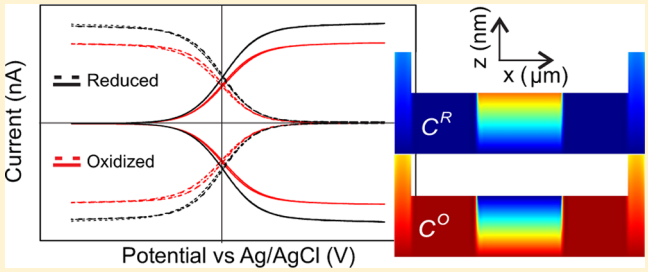

In electrochemical detection at micro- and nanoelectrodes,[1,2] where mass transport is commonly limited by diffusion, the measured current is proportional to the diffusion coefficient of the analyte species. This relationship can however become complex in redox cycling between two electrodes[3−6] due to unequal diffusivities of the oxidized and reduced forms of the analyte. This can influence both transient[7−11] and steady-state[12−14] behavior of the current. It is therefore crucial to understand the effect of unequal diffusivities of the oxidized and the reduced species for a quantitative interpretation of redox-cycling measurements.

A well-studied case is scanning electrochemical microscopy (SECM).[15−17] Due to unequal diffusivities, the steady-state current in SECM depends on the mode of operation:[8] interchanging the potentials of the tip and the substrate, that is, switching between the feedback mode[7,18,19] and the substrate generation/tip collection (SG/TC) mode,[8,20,21] changes the steady-state current by a factor equal to the ratio of the diffusivities of the oxidized and the reduced species. Martin and Unwin[7,8] performed a detailed numerical study of these effects supported by experiments for the SECM geometry (a shrouded disk microelectrode in close proximity to a planar substrate). This geometry has the particular feature that the bias of the substrate (reducing or oxidizing) also determines the species present in the "bulk" solution surrounding the microelectrode. For example, if the substrate is biased at an oxidizing potential, then the solution in the region surrounding the microelectrode, which is part of the one-dimensional diffusion zone generated by the substrate electrode, becomes essentially fully oxidized over time, independently of whether reduced or oxidized molecules were present in the original solution. This property was exploited in the experiments of Martin and Unwin to create a "bulk" solution of oxidized species. More recently, several experiments have started focusing on experimental geometries where this coupling between one of the electrodes and bulk does not exist. These include for example experiments where the conducting substrate is limited in extent, as studied by Zoski et al.[22] and more recently by Oleinick et al.,[23] as well as microfabricated nanogap devices that are only weakly coupled to bulk solution, as investigated by our group.[24] In these situations, the nature of the bulk solution and the polarity of the electrode biases can be independently controlled, in which case conclusions of refs 7 and 8 may not directly apply.

Here we investigate this question using nanogap devices,[24] in which the active region where redox cycling takes place is only weakly coupled to a bulk reservoir. This allows us to study independently the effect of switching the modes of operation and the influence of the species in the bulk. We observe that it is not the mode of operation but rather the redox state of the species in the bulk solution that controls the current during redox cycling. By using straightforward theoretical arguments, which are further supported by numerical calculations, we quantitatively explain these experimental findings.

This article is organized as follows. We first present numerical simulations based on diffusive mass transport and the detailed specific geometry relevant in our experiments. We then derive analytical expressions for the diffusion-limited current that reproduce the full numerical result. These relatively simple expressions are more general than the numerical results in that they also apply to other geometries. Finally, we validate both numerical and analytical results through direct comparison with experiments.

Received: March 27, 2013
Accepted: May 15, 2013
Published: May 15, 2013

   dx.doi.org/10.1021/ac400910n | *Anal. Chem.* 2013, 85, 6053−6058

NUMERICAL MODEL

We consider a simple outer-sphere heterogeneous electron-transfer reaction at the electrodes, O + $ne \rightleftharpoons$ R, where n is the number of electrons transferred. Following the approach of Martin and Unwin,[7,8] we numerically evaluate the diffusion-limited current under redox-cycling conditions for the general case where the diffusion coefficients for the reduced and the oxidized forms of a redox couple (D^R and D^O, respectively) have different values. We assume that the supporting electrolyte concentration is much greater than that of the redox species. Under these conditions, steady-state mass transport obeys the diffusion equation

$$\nabla^2 C^{R,O} = 0 \tag{1}$$

where C^R and C^O represent the concentrations of the reduced and the oxidized forms, respectively. The corresponding fluxes are given by

$$j^{R,O} = -D^{R,O}\nabla C^{R,O} \tag{2}$$

We solved eq 1 for both R and O using a finite-element simulation (COMSOL Multiphysics 4.2), as reported earlier.[26] The simulation was performed over a two-dimensional domain representing the geometry and dimensions of the nanogap devices employed in our experiments, as sketched in Figure 1.

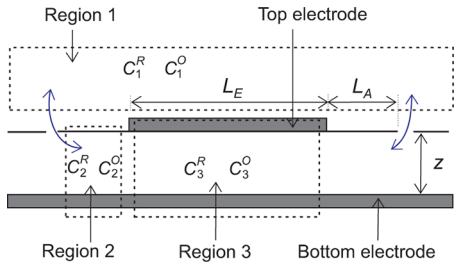

Figure 1. Schematic illustration of the device geometry employed for numerical simulations. Also shown are the three regions employed in analytical calculations: region 1, the bulk solution outside the device; region 2, the access channel without redox cycling; and region 3, the active region of the device where redox cycling takes place.

In short, the devices consist of two electrodes separated by a distance z = 60 nm. The top electrode has a length L_E = 10 μm and defines the so-called active region of the device. The active region is connected at both ends to outside reservoirs via nanochannels of length L_A = 8 μm and of the same height as the active region, z. The bottom electrode spans the entire length of the device, including both the active region and the access channel. Note that, importantly for the conclusions drawn below, the dimensions of the device satisfy the conditions $z \ll L_E$, L_A. For simplicity, we assume that the electrodes span the whole width of the channel in the third (out of the page) dimension; the solution is then uniform in this third dimension and the simulations can be performed and represented in only two dimensions. Boundary conditions corresponded to a high reducing overpotential at one electrode and a high oxidizing overpotential at the other electrode (reducing electrode: $C^O = 0$ and $j^R = -j^O$; oxidizing electrode: $C^R = 0$ and $j^O = -j^R$). The diffusion coefficients of the reduced and the oxidized molecules in aqueous solution were taken as 6.7×10^{-10} m^2/s and 5.36×10^{-10} m^2/s, respectively, corresponding to the experimental conditions reported below and to a diffusion coefficient ratio $\gamma = D^O/D^R = 0.8$.[8] The concentrations in the bulk solution far from the entrances to the device, C_1^O and C_1^R, were treated as constant.

The results of the numerical simulations are summarized in Figure 2. We distinguish between four cases depending on whether the top or the bottom electrode is the reducing electrode and on whether the bulk solution contains only R ($C_1^R = C_B$, $C_1^O = 0$) or only O ($C_1^O = C_B$, $C_1^R = 0$).

Figure 2a shows the two-dimensional concentration profiles $C^{R,O}(x,z)$ for the case where the bulk contains reduced species and the bottom electrode is oxidizing. Under these conditions, there exists a concentration gradient between the bulk solution and the access channel (regions 1 and 2 in Figure 1) since the bottom electrode oxidizes molecules from the bulk. There is also an approximately spherical concentration gradient extending into the bulk solution near each access hole of the device, but this lies outside the domain shown in Figure 2a. In the access channel region, on the other hand, essentially all molecules are in the oxidized form due to the intimate contact with the bottom electrode. Finally, in the active region redox cycling causes steep gradients of both reduced and oxidized species between the electrodes. These gradients in the z-direction are essentially independent of x except for a short transition zone (length a few times z) at each end of the active region. Because $z \ll L_E$, this transition zone represents only a small perturbation on the total redox cycling flux.

Figure 2b shows the one-dimensional concentration profiles $C^{R,O}(0,z)$ in the z-direction at a location halfway between the access holes (corresponding to the cross section lines in the active region in panel a). As required by the boundary conditions, the concentration of R is maximal at the reducing electrode and vanishes at the oxidizing electrode; the converse is true for O. Both concentration gradients are linear, reflecting the fact that, apart from a small region near the edges of the active region, the diffusion gradient is effectively one-dimensional between the electrodes. The maximum concentration of R is simply the bulk concentration, C_B, while the concentration of R averaged in the z-direction over the height of the device, which we denote by $\overline{C}_3^R$, is $C_B/2$. The concentration of O, on the other hand, is modified by a factor of $1/\gamma = 1.25$ compared to that of R, such that $\overline{C}_3^O = C_B/2\gamma$. This difference between $\overline{C}_3^R$ and $\overline{C}_3^O$ is dictated by the electrode boundary condition $j^R = -j^O$: since $j^{R,O} = \pm 2D^{R,O}\overline{C}_3^{R,O}/z$, this boundary condition reduces to

$$\overline{C}_3^O = \frac{D^R}{D^O}\overline{C}_3^R = \frac{\overline{C}_3^R}{\gamma} \tag{3}$$

It further follows from the above that the total concentration of redox species in the active region is given by $\overline{C}_3^R + \overline{C}_3^O = C_B(1 + 1/\gamma)/2$, which differs from the bulk concentration when $\gamma \neq 1$. This is possible because there exists a connection to the bulk reservoir and could not occur in a sealed volume. The total faradaic current corresponding to eq 3 is given by

$$i_{lim}^R = nFA|j^R| = nFA|j^O| = \frac{nFAD^R C_B}{z} \tag{4}$$

where F is the Faraday constant and A the area of overlap between the electrodes. This is the same result as if the diffusion coefficient for O had been ignored entirely; this is because the different speed of diffusion of O is compensated by the changes in concentration observed in Figure 2.

Figure 2c shows the R and O concentration profiles in the active region for a different case, namely, where the bulk

dx.doi.org/10.1021/ac400910n | Anal. Chem. 2013, 85, 6053−6058

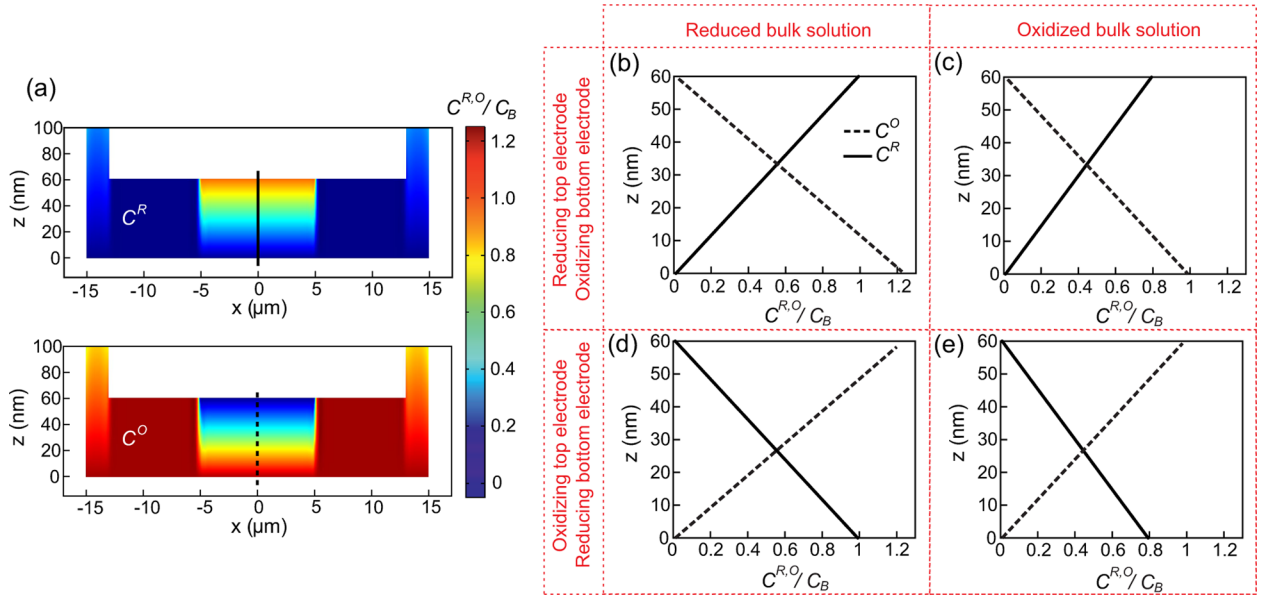

Figure 2. Results of numerical calculations. (a) Concentrations of R (top panel) and O (bottom panel) under steady-state conditions for the case where the bottom electrode is oxidizing, the top electrode reducing, and the bulk solution outside the device contains only R. The highly skewed aspect ratio is for clarity. (b–e) One-dimensional concentration profiles $C^{R,O}(x = 0,z)$ along the cross-section lines in panel (a). The cases where the top electrode is reducing and the bottom electrode is oxidizing are shown in the top row (panels b, c), while results for the opposite bias condition are shown in the bottom row (panels d, e). Both cases with reduced (panels b, d) and oxidized (panels c, e) species in the bulk reservoir are shown. All concentrations are normalized to the concentration of species in the reservoir, C_B.

solution is in the oxidized form instead of the reduced form. The profiles are qualitatively similar to those of panel b, except that the concentrations are modified by a factor γ: we now observe $\overline{C}_3^O = C_B/2$ and $\overline{C}_3^R = \gamma C_B/2$. The corresponding change in gradients leads to a corresponding change in faradaic current,

$$i_{\lim}^{O} = \frac{nFAD^{O}C_B}{z} = \gamma i_{\lim}^{R} \tag{5}$$

Finally, Figure 2d and e shows the corresponding profiles when the roles of the electrodes (reducing or oxidizing) are inverted. The only change in the concentration profiles is that they are inverted in the z direction, reflecting the inverted roles of the top and bottom electrodes; the magnitudes of the concentration gradients are unaffected. Correspondingly, the faradaic current is also unaffected. This indicates that it is the species present in the bulk that influences the diffusion-limited current rather than the choice of which electrode is reducing or oxidizing.

■ ANALYTICAL MODEL

While useful for gaining a detailed understanding of the factors at play, results from numerical simulations are by their very nature obtained for a specific geometry and it is not necessarily clear how generally we can apply the conclusions drawn from a particular set of simulations. Here, armed with insights gained from the numerical study, we derive a simple analytical theory that reproduces the predictions of the simulations. Importantly, however, the derivation is independent of the specific geometry of the nanogap, so long as some simple prerequisite conditions are satisfied. The analytical results can thus be employed for other redox cycling geometries without the need for additional numerical simulations for each case.

We first note that there exist three distinct regions in the system where the ratio of the concentrations of R and O is fixed, as illustrated in Figure 1. Region 1 consists in the bulk solution. Here the concentrations of R and O, C_1^R and C_1^O, respectively, are known by assumption. Region 2 consists of the part of the access channel far from both the active region and the access holes to bulk solution (where "far" signifies a distance of a few times the channel height, z). Here $C_2^O = \beta C_2^R$, where β is set by the potential of the bottom electrode; $\beta \to 0$ and $\beta \to \infty$ correspond to the bottom electrode being reducing or oxidizing, respectively. Finally, region 3 consists of the active region; here both $\overline{C}_3^R$ and $\overline{C}_3^O$ are finite during redox cycling, and their magnitudes are related by eq 3.

Between these three regions, there exist transition zones (with a spatial extent of the order of z) where significant gradients in C^R and C^O can occur in the x-direction. For example, for the case of Figure 2a, there is a diffusive flux of O from the access channels to the active region and a compensating flux of R in the opposite direction. Using the symbol J to represent the total flux integrated across the entire cross-section of the channel, this situation corresponds to $J_{2\to3}^O > 0$ and $J_{2\to3}^R < 0$. Under steady-state conditions, the total flux of redox molecules, either reduced or oxidized, must however vanish. Therefore

$$J_{p\to q}^{R} + J_{p\to q}^{O} = 0 \tag{6}$$

where p, q represent any pair of adjacent reservoirs.

In order to determine explicit expressions for the fluxes $J_{p\to q}^{R,O}$ for diffusive transport between the various regions, it is necessary to solve the diffusion equation, eq 1, for the specific geometry of interest. For our present purpose, however, it will prove sufficient that, without loss of generality, the expression for the total flux has the form[27]

$$J_{p\to q}^{R,O} = D^{R,O}(C_p^{R,O} - C_q^{R,O})b \tag{7}$$

Here b is a geometry-dependent constant with the units of length. Importantly the value of b is independent of the

dx.doi.org/10.1021/ac400910n | Anal. Chem. 2013, 85, 6053–6058

diffusion coefficient or concentration;[28] for a given geometry, its value is thus identical for R and O. Substituting eq 7 into the steady-state condition, eq 6, yields expressions relating the concentrations of R and O in region q to those in region p. Applying this procedure to the bulk solution (region 1) and the access channel (region 2) yields expressions for the concentrations in the access channel (averaged over the channel height)

$$\bar{C}_2^R = \frac{1}{1+\gamma\beta}(C_1^R + \gamma C_1^O) \tag{8}$$

and

$$\bar{C}_2^O = \frac{\beta}{1+\gamma\beta}(C_1^R + \gamma C_1^O) \tag{9}$$

Repeating the procedure between regions 2 and 3 and using eq 8 and eq 9 to eliminate $\bar{C}_2^R$ and $\bar{C}_2^O$ then yields the concentrations in the active region in terms of those in the bulk

$$\bar{C}_3^R = \frac{C_1^R + \gamma C_1^O}{2} \tag{10}$$

and

$$\bar{C}_3^O = \frac{C_1^R + \gamma C_1^O}{2\gamma} \tag{11}$$

Equation 10 and eq 11 can be used to obtain $|j^R|$ and $|j^O|$, respectively. Following a similar procedure as in eq 4, the corresponding diffusion-limited current is

$$i_{lim} = \frac{nFAD^R}{z}(C_1^R + \gamma C_1^O) \tag{12}$$

Interestingly, this result is independent of the parameter β characterizing the access channel; indeed, it can also be obtained by applying eq 6 to regions 1 and 3 directly.

Equation 12 is valid for any mixture of R and O in the bulk solution; for the special cases of fully reduced ($C_1^R = C_B$ and $C_1^O = 0$) and fully oxidized ($C_1^R = 0$ and $C_1^O = C_B$) bulk solution, it reduces to eq 4 and eq 5, respectively. Importantly, the equation, since derived from eq 7, is independent of the specific geometry and applies equally well to other systems where redox cycling takes place. The only requirements for its validity are that (1) the electrodes are much closer together than the lateral dimensions of the electrodes ($z \ll L_E$ in our particular geometry; $z \ll$ electrode radius for a shrouded disc electrode as in SECM), and (2) there is a sufficiently large overpotential that complete reduction or oxidation occurs at the two electrodes. Equation 12 is in this sense far more general than the results of the simulations of the previous section.

Finally, we note that, while the derivation above focused solely on the diffusion-limited current, it is straightforward to generalize it to the whole voltammogram so long as the heterogeneous reaction kinetics are reversible. The result in this case is simply that the whole voltammogram scales with C_1^R and C_1^O in the same manner as the limiting current, as described above. For the case of quasireversible kinetics, on the other hand, a more complex calculation would be required for values of the potential in the vicinity of the half-wave potential; such a calculation lies beyond the scope of the present work.

EXPERIMENTAL METHODS

Potassium chloride, 1,1-ferrocene dimethanol and ammonium persulphate ($(NH_4)_2S_2O_8$) were obtained from Sigma-Aldrich in analytical grade and used without further purification. Chromium etchant was obtained commercially from Transene Co. Inc. Deionized and filtered water was obtained from a Milli-Q Advantage ultrapure water system. One Molar KCl (Sigma-Aldrich) was used as supporting electrolyte.

To prepare solutions with fully oxidized redox species, 50 μL of 100 mM $(NH_4)_2S_2O_8$ was added to 10 mL of a 1 mM 1,1-ferrocene dimethanol aqueous solution purged with nitrogen for 10 min. Cyclic voltammetry at an ultramicroelectrode was employed to verify that the solution was fully oxidized.

The nanogap device was fabricated on a silicon substrate employing techniques reported previously[24,25] except that photolithography was employed instead of electron-beam lithography. The fabricated devices contained two Pt electrodes separated by a Cr sacrificial layer of thickness 60 nm. The bottom electrode was 3 μm in width and 22 μm in length. The top electrode was 9 μm in width and 10 μm in length. The active region of the device was defined as the volume encompassed by the overlapping top and bottom electrodes (3 μm × 10 μm × 60 nm). The access holes were located at the top of the device, 8 μm away from the ends of the top electrode. Directly before the measurements, the sacrificial layer was chemically removed using a wet chromium etch at room temperature, thus forming the nanochannel. The etching procedure was monitored electrically by measuring the resistance between the top and bottom electrodes.

Electrochemical experiments in the nanogap devices were performed with two Keithley 6430 subfemtoampere source meters used both as voltage sources to bias the electrode potentials and as current meter. The Keithley instruments were controlled remotely using custom Labview code. Electrochemical measurements using a polished carbon ultra micro electrode (UME) of radius 5.5 μm (BASi MF-2007) were performed with a bipotentiostat (CHI832B, CH Instruments). For all the measurements the potentials were applied with respect to a 3 M Ag/AgCl reference electrode (BASi, Figure 3). No auxiliary electrode was used in either case due to the low current level through the reference electrode. All the experiments were carried out at room temperature (21 ± 2 °C).

EXPERIMENTAL RESULTS

We started with measuring the cyclic voltammetry of the 1,1-ferrocene dimethanol solution using a carbon UME, as shown in Figure 4 (black curve). The electrode potential was swept between 0 and 0.5 V vs Ag/AgCl and a sigmoidal oxidation wave was observed with half wave potential E_0 = 0.24 V, as expected for 1,1-ferrocene dimethanol. The corresponding voltammorgram for 1,1-ferrocene dimethanol in the oxidized form is also shown in Figure 4 (red curve), where a reduction wave is now observed. The limiting currents for the cases of bulk solution with R (black curve) and O (red curve) species are proportional to D^R and D^O, respectively. Therefore, the ratio of the wave heights of the two curves in Figure 4 gives the diffusivity ratio, $\gamma = D^O/D^R$. Our data yield γ = 0.80 ± 0.01, which is closely comparable to the values reported in the literature.[8]

Immediately following the UME experiments, we performed measurements in nanogap devices using the same solutions. The devices were filled with solution containing only reduced

dx.doi.org/10.1021/ac400910n | Anal. Chem. 2013, 85, 6053−6058

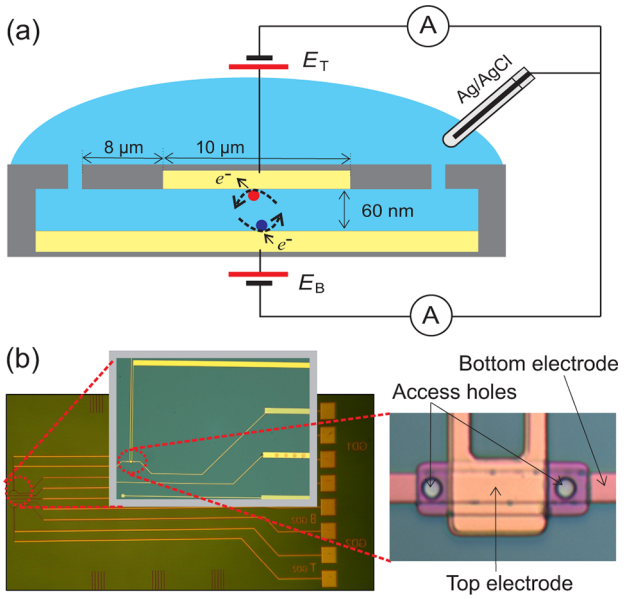

Figure 3. (a) Schematic diagram of the experimental configuration. (b) Top view optical images of a device with the zoomed in part showing the nanogap region.

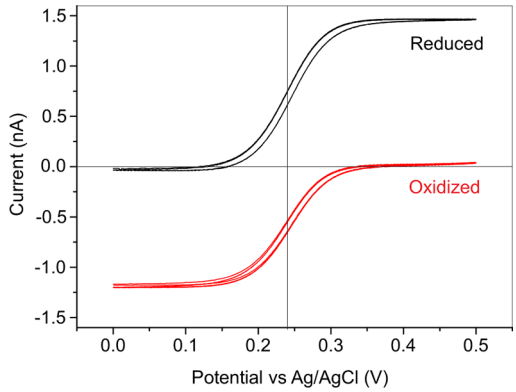

Figure 4. Cyclic voltammograms using a carbon UME for 1,1-ferrocene dimethanol solution in the reduced form (black curve) and the oxidized form (red curve). The ratio of the limiting currents in the two voltammograms yields the ratio of the diffusion coefficients, $\gamma = D^O/D^R$. Scan rate 20 mV/s.

species. The top electrode was scanned from 0 to 0.5 V vs Ag/AgCl while keeping the bottom electrode at a reducing potential (0 V) or an oxidizing potential (0.5 V). The former configuration corresponds to the feedback mode and the latter to the SG/TC mode in SECM. The measured voltammograms for the two scanning modes are shown in Figure 5 (black curves). The figure includes voltammograms for both the top and the bottom electrodes; the curves are essentially identical except for a sign reversal in the current, as expected for redox cycling. Contrary to SECM studies,[7,8] the limiting current is independent of which electrode is reducing or oxidizing. As discussed above, we attribute this difference to the fact that here the coupling between the bottom electrode and the bulk reservoir is weak enough that the composition of the bulk remains essentially unaffected by reactions taking place in the nanogap device.

The same set of experiments was repeated using the solution containing ferrocene in the oxidized form. The measured curves are also shown in Figure 5 (red curves). Again, the steady-state

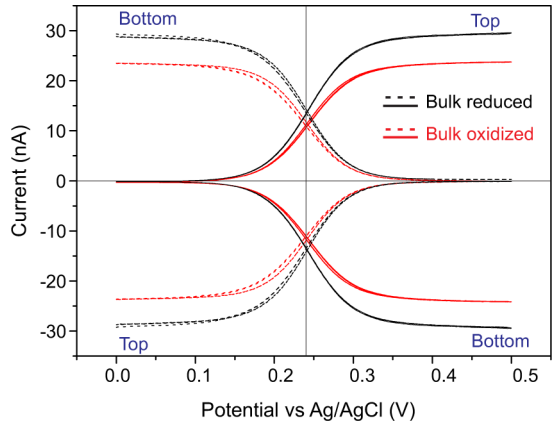

Figure 5. Cyclic voltammograms for a nanogap device. The bottom electrode is kept at a reducing (solid lines) or oxidizing (dashed lines) potential while the top electrode is swept. The solution in the bulk solution outside the device contained 1,1-ferrocene dimethanol in either the reduced (black lines) or oxidized (red lines) form. The current at both electrodes is shown for each case, as identified by the labels "Top" and "Bottom". The limiting current is independent of which electrode is reducing or oxidizing but is systematically lower by a factor 0.83 ± 0.03 when the bulk solution is in the oxidized form (red lines). Scan rate 20 mV/s.

current is independent of choice of which electrode is reducing or oxidizing, that is, of the mode of operation. The limiting current is however decreased compared to the case with reduced molecules in the bulk solution (black curves) in a manner reminiscent of the UME measurements. The measured ratio of the limiting currents for the two cases is 0.83 ± 0.03. Equation 4 and eq 5 predict that this ratio should correspond to the diffusivity ratio, γ. This is fully consistent with the value of this ratio determined from the UME measurements, $\gamma = 0.80 \pm 0.01$.

SUMMARY

In summary, we have derived a general expression, eq 12, for the diffusion limited current in redox cycling. We have shown theoretically that eq 12 is valid for any mixture of R and O species in the bulk solution and independent of the geometry of the redox cycling device. Our theoretical results indicate that the diffusion-limited current is influenced by the redox state of the species in the surrounding bulk solution and not by the choice of which electrode is reducing or oxidizing. These predictions were tested experimentally using microfabricated nanogap electrodes and good quantitative agreement was found. Our results provide a straightforward way of eliminating possible systematic errors due to unequal diffusion coefficients in a broad range of redox cycling systems.

For the specific case of the SECM configuration, it was instead reported earlier that the choice of which electrode is reducing or oxidizing influences the current.[7,8] There is no contradiction with the present conclusions, however, since in the SECM case the contents of the "bulk" solution near the tip electrode is determined by the bias of the macroscopic working electrode and is not an independently controlled parameter as in the general case discussed here.

dx.doi.org/10.1021/ac400910n | Anal. Chem. 2013, 85, 6053−6058

AUTHOR INFORMATION

Corresponding Author

*E-mail: s.g.lemay@utwente.nl. Phone: +31 53 489 2306. Fax: +31 53 489 3511.

Notes

The authors declare no competing financial interest.

ACKNOWLEDGMENTS

We gratefully acknowledge the assistance of H. A. Heering for the protocol for preparing oxidized ferrocene solutions. Financial support was provided by The Netherlands Organization for Scientific Research (NWO) and the European Research Council (ERC).

REFERENCES

(1) Privett, B. J.; Shin, J. H.; Schoenfisch, M. H. *Anal. Chem.* **2010**, *82*, 4723−4741.
(2) Kimmel, D. W.; Leblanc, G.; Meschievitz, M. E.; Cliffel, D. E. *Anal. Chem.* **2012**, *84*, 685−707.
(3) Bard, A. J.; Mirkin, M. V.; Unwin, P. R.; Wipf, D. O. *J. Phys. Chem.* **1992**, *96*, 1861−1868.
(4) Niwa, O.; Xu, Y.; Halsall, H. B.; Heineman, W. R. *Anal. Chem.* **1993**, *65*, 1559−1563.
(5) Schienle, M.; Paulus, C.; Frey, A.; Hofmann, F.; Holzapfl, B.; Bauer, P. S.; Thewes, R. *IEEE J. Solid-State Circuits* **2004**, *39*, 2438−2445.
(6) Kätelhön, E.; Hofmann, B.; Lemay, S. G.; Zevenbergen, M. A. G.; Offenhäusser, A.; Wolfrum, B. *Anal. Chem.* **2010**, *82*, 8502−8509.
(7) Martin, R. D.; Unwin, P. R. *J. Electroanal. Chem.* **1997**, *439*, 123−136.
(8) Martin, R. D.; Unwin, P. R. *Anal. Chem.* **1998**, *70*, 276−284.
(9) Amatore, C.; Sella, C.; Thouin, L. *J. Phys. Chem. B* **2002**, *106*, 11565−11571.
(10) Zoski, C. G.; Luman, C. R.; Fernández, J. L.; Bard, A. J. *Anal. Chem.* **2007**, *79*, 4957−4966.
(11) Ghilane, J.; Lagrost, C.; Hapiot, P. *Anal. Chem.* **2007**, *79*, 7383−7391.
(12) Oldham, K. B. *Anal. Chem.* **1996**, *68*, 4173−4179.
(13) Hyk, W.; Stojek, Z. *Anal. Chem.* **2002**, *74*, 4805−4813.
(14) Hyk, W.; Stojek, Z. *Anal. Chem.* **2005**, *77*, 6481−6486.
(15) Bard, A. J.; Fan, F. R. F.; Kwak, J.; Lev, O. *Anal. Chem.* **1989**, *61*, 132−138.
(16) Kwak, J.; Bard, A. J. *Anal. Chem.* **1989**, *61*, 1221−1227.
(17) Bard, A. J.; Fan, F. R. F.; Pierce, D. T.; Unwin, P. R.; Wipf, D. O.; Zhou, F. *Science* **1991**, *254*, 68−74.
(18) Lee, C.; Kwak, J.; Anson, F. C. *Anal. Chem.* **1991**, *63*, 1501−1504.
(19) Amemiya, S.; Bard, A. J.; Fan, F. R. F.; Mirkin, M. V.; Unwin, P. R. *Annu. Rev. Anal. Chem.* **2008**, *1*, 95−131.
(20) Engstrom, R. C.; Meaney, T.; Tople, R.; Wightman, R. M. *Anal. Chem.* **1987**, *59*, 2005−2010.
(21) Martin, R. D.; Unwin, P. R. *J. Chem. Soc., Faraday Trans.* **1998**, *94*, 753−759.
(22) Zoski, C. G.; Simjee, N.; Guenat, O.; Koudelka-Hep, M. *Anal. Chem.* **2004**, *76*, 62−72.
(23) Oleinick, A. I.; Battistel, D.; Daniele, S.; Svir, I.; Amatore, C. *Anal. Chem.* **2011**, *83*, 4887−4893.
(24) Zevenbergen, M. A. G.; Krapf, D.; Zuiddam, M. R.; Lemay, S. G. *Nano Lett.* **2007**, *7*, 384−388.
(25) Zevenbergen, M. A. G.; Wolfrum, B. L.; Goluch, E. D.; Singh, P. S.; Lemay, S. G. *J. Am. Chem. Soc.* **2009**, *131*, 11471−11477.
(26) Rassaei, L.; Mathwig, K.; Goluch, E. D.; Lemay, S. G. *J. Phys. Chem. C* **2012**, *116*, 10913−10916.
(27) Singh, P. S.; Goluch, E. D.; Heering, H. A.; Lemay, S. G. *Applications of Electrochemistry and Nanotechnology in Biology and Medicine II, volume 53 of Modern Aspects of Electrochemistry*; Eliaz, N. Ed.; Springer: New York, 2012; pp 1−66.
(28) Oldham, K. B. *J. Electroanal. Chem.* **1992**, *323*, 53−76.